Article

High-Resolution Topographic and Chemical Surface Imaging of Chalk for Oil Recovery Improvement Applications

Tine Vigdel Bredal [1,2,*], Udo Zimmermann [1,2], Merete Vadla Madland [3], Mona Wetrhus Minde [2,4], Alexander D. Ost [5,6], Tom Wirtz [5], Jean-Nicolas Audinot [5] and Reidar Inge Korsnes [1,2]

1 Department of Energy Resources, University of Stavanger, Ullandhaug, 4036 Stavanger, Norway; udo.zimmermann@uis.no (U.Z.); reidar.i.korsnes@uis.no (R.I.K.)
2 The National IOR Centre of Norway, University of Stavanger, Ullandhaug, 4036 Stavanger, Norway; mona.w.minde@uis.no
3 Division of Research, University of Stavanger, Ullandhaug, 4036 Stavanger, Norway; merete.v.madland@uis.no
4 Department of Mechanical and Structural Engineering and Materials Science, University of Stavanger, Ullandhaug, 4036 Stavanger, Norway
5 Advanced Instrumentation for Nano-Analytics, Department of Materials Research and Technology, Luxembourg Institute of Science and Technology, 4362 Esch-sur-Alzette, Luxembourg; alexander.ost@list.lu (A.D.O.); tom.wirtz@list.lu (T.W.); jean-nicolas.audinot@list.lu (J.-N.A.)
6 Faculty of Science, Technology and Medicine, University of Luxembourg, 2 Av. de l'Universite, 4365 Esch-sur-Alzette, Luxembourg
* Correspondence: tine.v.bredal@uis.no

Abstract: Chalk is a very fine-grained carbonate and can accommodate high porosity which is a key characteristic for high-quality hydrocarbon reservoirs. A standard procedure within Improved Oil Recovery (IOR) is seawater-injection which repressurizes the reservoir pore pressure. Long-term seawater-injection will influence mineralogical processes as dissolution and precipitation of secondary minerals. These secondary minerals (<1 micrometer) precipitate during flooding experiments mimicking reservoir conditions. Due to their small sizes, analysis from traditional scanning electron microscopy combined with energy dispersive X-ray spectroscopy is not conclusive because of insufficient spatial resolution and detection limit. Therefore, chalk was analyzed with high-resolution imaging by helium ion microscopy (HIM) combined with secondary ion mass spectrometry (SIMS) for the first time. Our aim was to identify mineral phases at sub-micrometer scale and identify locations of brine–rock interactions. In addition, we wanted to test if current understanding of these alteration processes can be improved with the combination of complementary imaging techniques and give new insights to IOR. The HIM-SIMS imaging revealed well-defined crystal boundaries and provided images of excellent lateral resolution, allowing for identification of specific mineral phases. Using this new methodology, we developed chemical identification of clay minerals and could define their exact location on micron-sized coccolith grains. This shows that it is essential to study mineralogical processes at nanometer scale in general, specifically in the research field of applied petroleum geology within IOR.

Keywords: helium ion microscopy; secondary ion mass spectrometry; chalk; clay mineral; chemistry; nano-scale imaging; mineralogical alteration

1. Introduction

Chalk is a marine sedimentary rock that comprises mainly calcium carbonate ($CaCO_3$) which is primarily composed of micron-sized coccolithophore fragments (coccoliths) and nano-sized fossil debris. The size of individual coccolith rings ranges between 0.3 and 5 µm [1]. Precipitation and deposition of chalk typically occur in deep marine settings, where clastic input is secondary if not absent. Accessory minerals may be silicate-rich microfossils or clay minerals related to aerial transport from volcanic eruptions. Due to the

characteristic texture of the chalk (Figure 1), the rock is also highly porous, nevertheless, its softness may cause compaction during diagenesis. This pronounced porosity is vital for the oil industry as it provides great potential as reservoirs for hydrocarbons. Water injection into carbonate reservoirs, such as the giant Ekofisk on the Norwegian Continental Shelf (NCF), is performed as a method known as Improved Oil Recovery (IOR) to gain more hydrocarbon from existing reservoirs instead of developing new fields [2–7]. This technique is essential in the transition process to a greener energy production in the future. The injected brine will alter the wettability of the grain surface from oil-wet to water-wet such that additional oil will be released [5]. However, this process will additionally alter the properties of the reservoir, initiate dissolution and precipitation of minerals, consequently influencing porosity and permeability [8–12]. Non-carbonate phases are suspected to influence the entire rock–fluid interaction and the identification is obviously the first step [11,13–16].
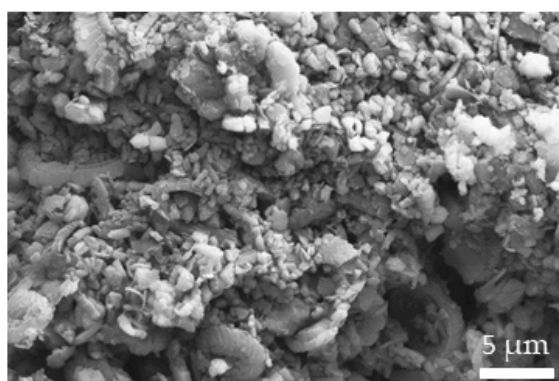

Figure 1. Typical texture of an Upper Cretaceous onshore chalk sample derived from the St. Vaast Formation from Obourg quarry close to Mons (Belgium; sample OBSV 12.3) imaged by SEM showing abundant coccolith rings and high porosity.

Magnesium is one of the most reactive ions in seawater. Seawater injection causes brine–rock interactions which normally involve calcium dissolution and magnesium precipitation. To identify secondary mineralogical and textural alteration of chalk, various methods of analytical tools have been applied [17]. The small size of these chalk constituents challenges the resolution of most of these techniques. Scanning Electron Microscopy (SEM) combined with elemental analysis using energy dispersive X-ray spectroscopy (EDS) is widely used on a regular basis for the purpose of performing reservoir characterization of chalk. This method can, however, not achieve sufficient spatial resolution and analytical sensitivity to resolve and identify mineral phases on sub-micron level as the acquired signal originates from an interaction volume of ~1 μm^3 in the sample [18,19]. Specific approaches within reservoir characterization on submicron scale needs state-of-the-art resolution in the field of imaging and mineral or component identification using crystallographic techniques or chemical data. The lack of these two data sets acquired at the same time, hampers the interpretation of mineralogical processes related to fluid injection as new grown minerals related t flooding experiments are in the nm size range [10,20,21]. The use of Transmission Electron Microscopy (TEM) has also been employed, however, sample preparation for this method is often challenging.

The main objective here is to provide high-resolution morphology images plus the mineral identification based on chemical surface analyses. Within three decades of IOR research we developed several methodological approaches to tackle this objective [17,22] (Minde et al., 2019a, b). Most of the analytical solutions turned out to be highly time consuming with significant challenges on sampling [20]. Crystallographic studies with tip-enhanced Raman spectroscopy (TERS) combined with atomic force microscopy (AFM) are extremely tedious and sample preparation is very challenging [22].

The novel combination of helium ion microcopy (HIM) with secondary ion mass spectrometry (SIMS) [23,24] allows to solve these issues for a variety of mineralogical and thus geological problems, especially in the field of rock–fluid interactions in IOR research. In the context of chalk analysis, we demonstrate in this manuscript for the first time the advantages of this method compared to those mentioned above and commence new and more advanced studies within this field.

2. Sample Material and Experimental Setup

The sample (OBSV 12) is Upper Cretaceous chalk from the St. Vaast Formation (Obourg quarry, Mons Belgium) [25–27]. The St. Vaast Formation has a high carbonate concentration with traces of glauconite, chlorite, and pyrite [28]. The chalk samples discussed here were cored with a cylindrical shape of 38.1 mm in diameter and a length of about 70 mm out of an un-weathered chalk block. A 2 mm drill bit was used to produce an artificial fracture without contaminating the sample. The size of the fracture aperture measured 2.25 mm ($\pm$0.05 mm) and ran parallel to the flooding direction in the central core (Figure 2a). The aim was to mimic fractured chalk in reservoirs such as Ekofisk on the NCS. In unflooded material the average amount of calcite was around 95% (Table 1). These cores were used for flooding experiments when different fluids were tested under reservoir conditions to provoke mineralogical changes which affect rock mechanics [29,30]. The main average abundances of the non-carbonate material (in weight percent) were SiO_2 (3.42 wt.%), followed by Al_2O_3 (1.01 wt.%), Fe_2O_3 (0.39 wt.%), and K_2O (0.23 wt.%) (Table 1). The experiment was conducted in a triaxial cell at high temperature (130 °C) with confining and pore pressure of 12 and 0.7 MPa, respectively. The test sample was initially flooded with NaCl during loading and the primary week during creep (deformation at constant stress) and was subsequently flooded for 53 days with synthetic seawater (SSW). The composition of this fluid is described in detail in [13] and comprises mainly sodium, chlorine, magnesium, calcium, potassium, and sulphur. For more information about the set-up of the triaxial cells, the reader is referred to [9]. The chalk sample was cleaned with distilled water after the experimental test, dried, and sliced into six units from OBSV 12.1 (inlet) to OBSV 12.6 (outlet).
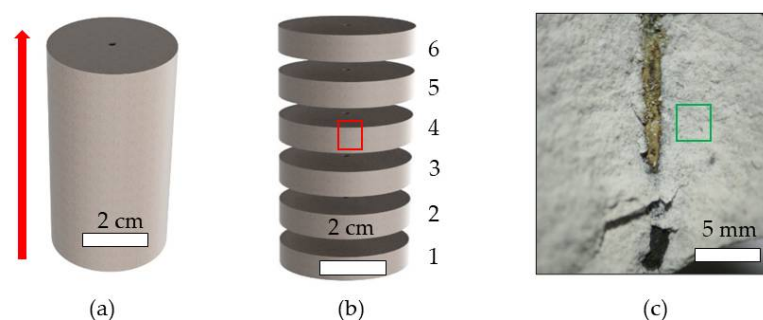

Figure 2. (**a**) The chalk sample (OBSV 12.4) before testing with the location of the drilled fracture (diameter: 2.25 $\pm$ 0.05 mm). The red arrow indicates the flooding direction. (**b**) The core was sliced after flooding, where number one is the "inlet", where the fluids were injected, and the "outlet" is number six. The red square in slice four shows the exact sample location for this study. (**c**) Optical microscopy image of the fracture fill from the sampling area after flooding of the sample. HIM-SIMS analysis was performed from sample material (green square) extracted from the matrix very close to the fracture fill.

Table 1. Bulk chemical composition of unflooded reference samples including the end piece of the flooded sample which has not been flooded (REF.6) and the flooded chalk samples of OBSV 12. Analysis with HIM-SIMS was performed on OBSV 12.4. wt.% indicates weight percent. The complete data set is available in Supplementary Table S1.

Content/ Sample	SiO_2 wt.%	Al_2O_3 wt.%	Fe_2O_3 wt.%	MgO wt.%	CaO wt.%	Na_2O wt.%	K_2O wt.%
REF.1	3.32	0.97	0.34	0.29	52.06	0.04	0.22
REF.2	3.39	1.00	0.54	0.27	51.90	0.04	0.22
REF.3	3.44	1.01	0.39	0.29	51.97	0.04	0.22
REF.4	3.38	1.00	0.34	0.28	52.29	0.04	0.22
REF.5	3.40	1.03	0.33	0.30	51.89	0.04	0.23
REF.6	3.58	1.05	0.40	0.28	51.89	0.04	0.24
OBSV 12#1	3.61	1.07	0.47	0.44	51.93	0.04	0.24
OBSV 12#2	3.52	1.05	0.38	0.48	52.05	0.04	0.22
OBSV 12#3	3.56	1.07	0.40	0.53	51.93	0.03	0.23
OBSV 12#4	3.64	1.08	0.43	0.52	51.88	0.04	0.22
OBSV 12#5	3.60	1.06	0.39	0.49	51.67	0.04	0.23
OBSV 12#6	3.62	1.08	0.43	0.40	51.94	0.04	0.24

3. Methods

3.1. Whole-Rock Geochemistry Characterization

In total, 5 g of sample material was milled in an agate mill to a fine mesh. The geochemical data were obtained by inductively coupled plasma–mass spectrometry (ICP-MS) analysis at ACME laboratory (Vancouver, BC, Canada). The milled sample was mixed with $LiBO_2/Li_2B_4O_7$ flux in crucibles and fused in a furnace. The cooled bead was dissolved in the American Chemical Society (ACS) grade nitric acid and analyzed by ICP-MS. Loss on ignition (LOI) was determined by igniting a sample split then measuring the weight loss. A 1 g sample was weighed into a tarred crucible and ignited to 1000 °C for 1 h, then cooled and weighed again. Total carbon and sulphur were determined using the LECO method. Here, induction flux was added to the prepared sample then ignited in an induction furnace. A carrier gas swept up released carbon to be measured by adsorption in an infrared spectrometric cell. Results are quantitative and give the concentrations of carbon and sulphur in all components. An additional 14 elements were measured after dilution in Aqua Regia. The prepared sample was digested with a modified Aqua Regia solution of equal parts concentrated HCl, HNO_3, and $DI-H_2O$ for 1 h in a heating block or hot water bath. The sample volume was increased with dilute HCl solution and splits of 0.5 g were analyzed. The accuracy and precision are between 2 and 3%.

3.2. Helium Ion Microscopy–Secondary Ion Mass Spectroscopy (HIM-SIMS)

Secondary electron (SE) image acquisitions were performed in a Zeiss ORION NanoFab Helium Ion Microscope (HIM) [31] (Figure 3). HIM uses a very finely focused He^+ or Ne^+ ion beam, produced by a gas field ion source (GFIS), to raster-scan the sample under investigation and to create SEs collected by an Everhart–Thornley (ET) detector. He^+ ions are typically used to produce SE images to limit sputtering of the surface during the imaging process due to the low sputtering yield of He^+ versus Ne^+ [32]. This gives spatial resolutions down to 0.5 nm [33,34] thanks to the high-brightness of the GFIS and the very small interaction volume between the impinging He^+ ions and the sample in the near surface region, from which SEs are emitted [31]. For more technical details about HIM the reader can refer to [24,31]. Chemical images were acquired by using a Secondary Ion Mass Spectrometer (SIMS) system installed on the HIM, which was developed by the Luxembourg Institute of Science and Technology (LIST) to provide analytical information of specimen on the HIM (called "HIM-SIMS") [23,24,33]. For SIMS, Ne^+ primary ions are used to enhance sputtering of the surface (up to a few nanometers of depth) and therefore to increase the secondary ion (SI) yield to achieve adequate signal statistics. The spatial resolution of the SIMS mode is better than 20 nm, which makes it a record in SIMS imaging [23,24].
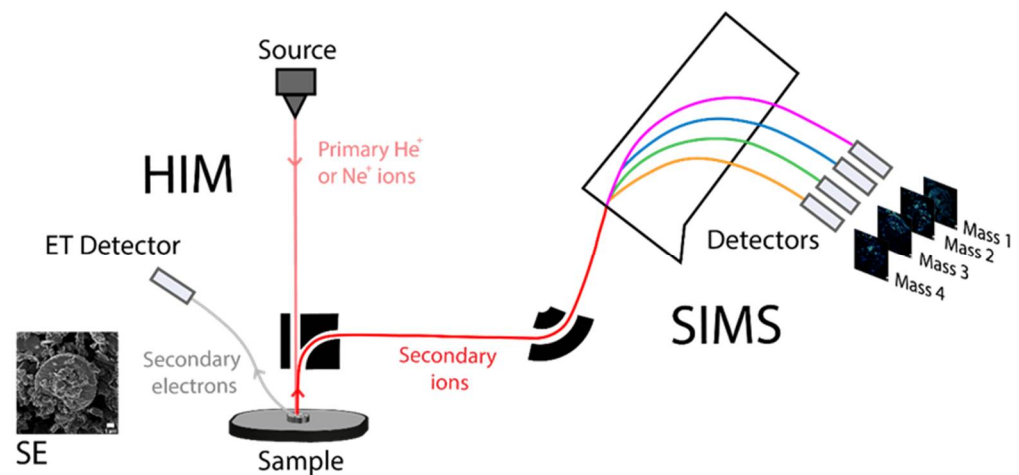
Figure 3. Schematic view of the HIM-SIMS instrument. The central part consists of the helium ion microscope (HIM) used primarily for topographic SE imaging, while the left part is showing the coupled secondary ion mass spectrometer (SIMS) add-on system dedicated for elemental analysis.

In situ analysis using both techniques, HIM for topographic SE imaging and SIMS for visualization of elemental distribution, firstly allows an efficient data acquisition workflow minimizing contamination of the sample and secondly facilitates image correlation of the same ROI in the data treatment process. Correlation of 2-dimensional topographic SE images and even 3D SE reconstructions using a photogrammetry method [35,36] and chemical images from SIMS, visualize complementary information in a single representation, thus enabling a deeper comprehension of a ROI with respect to its structural and chemical properties.

In this work, HIM-SE images were acquired with a He$^+$ primary current of 2 pA at 25 keV acceleration energy for a scanning of 2048 × 2048 pixels and a counting time of 10 μs/pixel averaged over 8 lines. For SIMS analysis, the surface of the same ROIs was scanned with a 10 pA (25 keV) Ne$^+$ beam with 512 × 512 pixels at a counting time of 2 ms/pixel. The instrument was tuned to map the distribution of the positive ion of magnesium (^{24}Mg$^+$), aluminum (^{27}Al$^+$), silicon (^{28}Si$^+$), potassium (^{39}K$^+$), and calcium (^{40}Ca$^+$) (^{24}Mg, ^{28}Si, ^{39}K in a first run and ^{27}Al and ^{40}Ca in a second run). The negative ions recorded were carbon (^{12}C$_2{}^-$) and oxygen (^{16}O$^-$).

4. Results

4.1. Geochemical Bulk Data

Bulk analysis results were acquired from un-flooded end pieces (where the endpiece of OBSV 12 is REF.6) and six flooded units of OBSV 12 (Table 1). The sample experienced an increase in magnesium concentration from 0.28 wt.% in the unflooded sample to 0.52 wt.% for OBSV 12.4 flooded with SSW. However, no significant loss of other elements was observed.

4.2. Helium Ion Microscopy Combined with Secondary Ion Mass Spectrometry (HIM-SIMS)

The HIM provided a high-resolution secondary electron (SE) image of a fresh surface chalk sample with detailed topographical features of the coccolith grains (Figure 4a). Elemental maps of the same ROI were acquired using SIMS (Figure 4b–h). ^{40}Ca was found correspondingly to the occurrence of the coccolith (Figure 4a), along with ^{12}C$_2$ and ^{16}O which shows the calcite (CaCO$_3$) distribution. However, there are a few locations on the coccolith surface where these ions are not detected: ^{24}Mg, ^{27}Al, ^{28}Si, and ^{39}K are distributed in areas of less than 1 μm^2, coinciding with the absence of ^{16}O, ^{40}Ca, and partly ^{12}C$_2$ signals (Figure 4e–h).
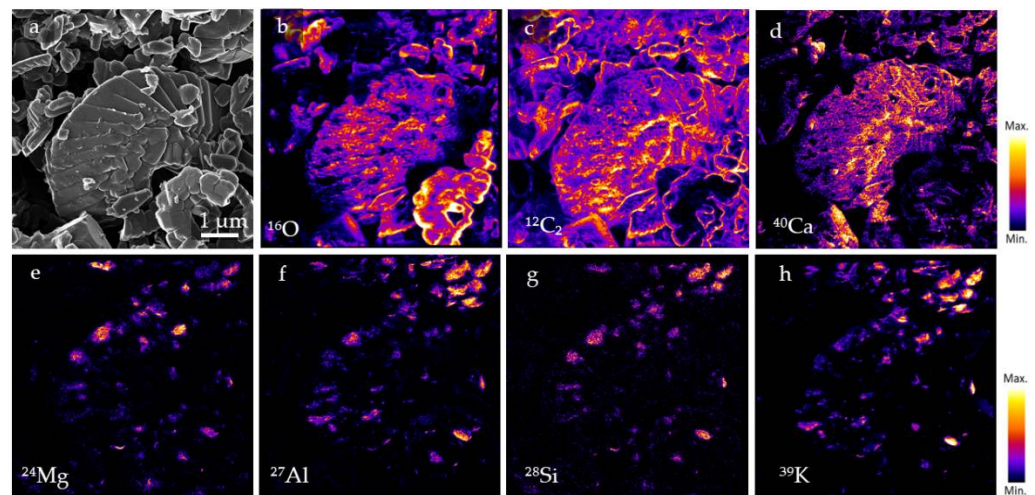
Figure 4. HIM-SIMS images of sample OBSV 12.4. (**a**) SE image of a ROI obtained by HIM focusing on a coccolith fragment. (**b–d**) Chemical images obtained by SIMS of ^{16}O, ^{12}C$_2$, and ^{40}Ca are presented with a scalebar at the right, representing the intensity of each element. (**e–h**) Elemental distribution of ^{24}Mg, ^{27}Al, ^{28}Si, and ^{39}K.

Separate clay grains were not identified in the selected SE image. An SE image overlayed with the SIMS maps of ^{24}Mg, ^{27}Al, ^{28}Si, and ^{39}K, in red, clearly defines locations and topography of clay coating the coccolith surface (Figure 5a). Increased magnification of the SE image allowed us to observe various surface roughness (Figure 5b,d,f) and the corresponding distribution of calcite in Figure 5c,e,g.
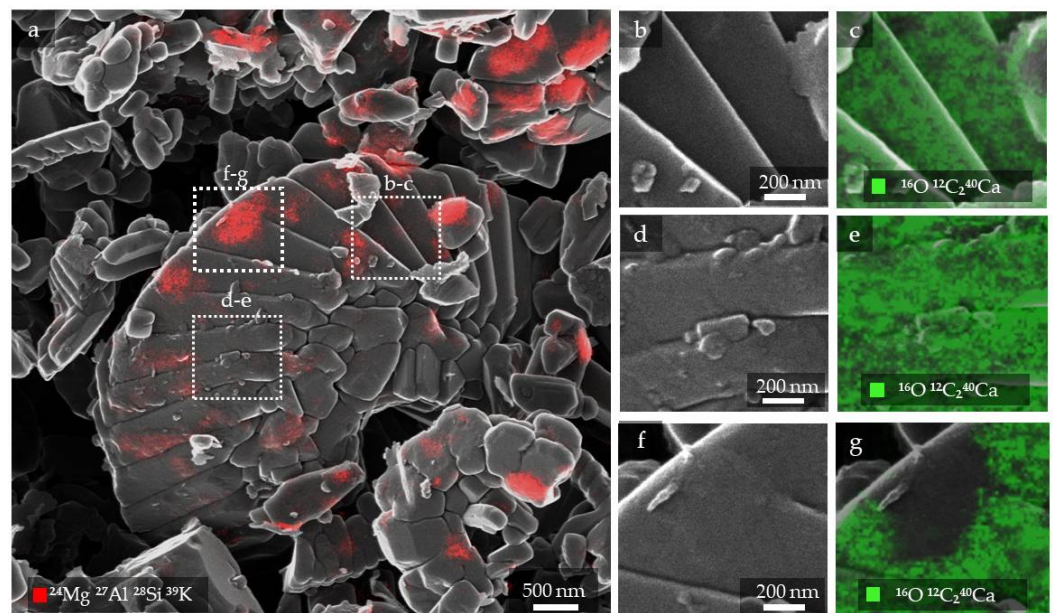

Figure 5. SE images with identified calcite distribution versus clay coating linked to topography of the coccolith grain and fragments. (**a**) The SE image is overlayed by the coinciding distribution of ^{24}Mg, ^{27}Al, ^{28}Si, and ^{39}K in red, representing clay. Three white boxes are marked and presented with increased magnification to highlight surface topography versus chemistry (**b–g**). (**b**) Smooth, yet stepwise surface (**c**) with distribution of ^{16}O, ^{12}C$_2$, and ^{40}Ca in green combined with the corresponding SE image. (**d**) Irregular surface. (**e**) The irregular surface in (**d**) is identified as calcite. (**f**) SE image with smooth surface which covers and evens out the steplike structure. (**g**) The overlay of (**f**) with the SIMS image presents a calcite dominated background.

Two clay minerals with different shapes on the same ROI were magnified to highlight possible compositional differences. A clay mineral was coating the surface and the second had a sheetlike appearance (Figures 6a–d and 6e–h). The second clay was thicker and lacked calcite distribution in the center. The ^{24}Mg concentration versus ^{27}Al, ^{28}Si and ^{39}K reflected a higher ^{24}Mg concentration on the sheetlike clay (Figure 6e–h).
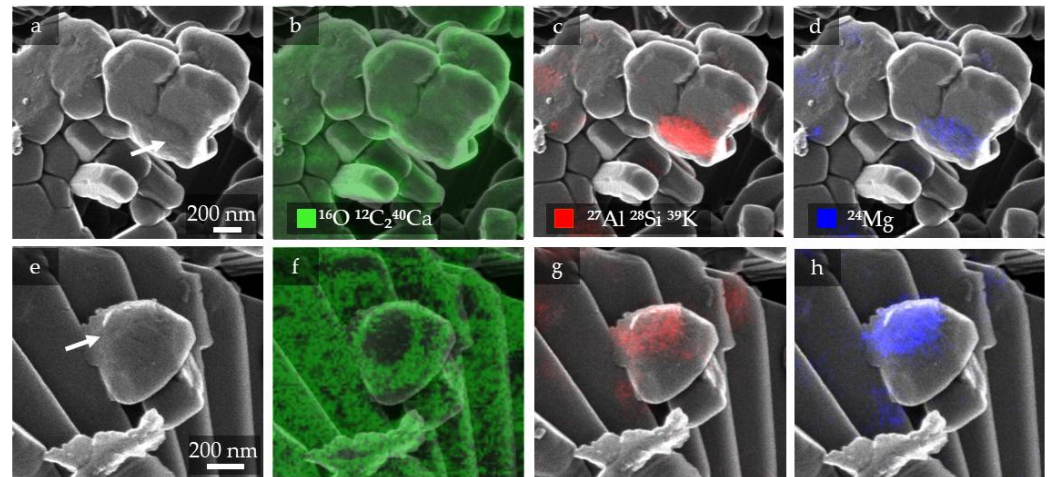

Figure 6. Series of SE and overlay of SE with SIMS results showing mineral phases of coccolith fragments and coating mineral phases, highlighting ^{24}Mg distribution. (**a**) SE image of a coccolith fragment highlighting a location with a slightly different roughness marked by a white arrow. (**b**) Calcite distribution (^{16}O, ^{12}C$_2$, and ^{40}Ca) overlaying the corresponding SE image. (**c**) SIMS detection of ^{27}Al, ^{28}Si, and ^{39}K overlapped with the corresponding SE image. These elements form a sub-micron phase of clay. (**d**) ^{24}Mg distribution. (**e**) SE image discloses a sheetlike feature covering a fragment marked by an arrow. (**f**) SIMS identification of calcite (^{16}O, ^{12}C$_2$, and ^{40}Ca) distribution, overlapping the corresponding SE image. Central absence of calcite. (**g**) The sheetlike mineral has presence of ^{27}Al, ^{28}Si, and ^{39}K representing clay. (**h**) ^{24}Mg is abundant on the sheetlike feature.

5. Discussion

High resolution imaging of chalk by HIM reveals detailed textural information of nanosized grains or coating adhered to the surface of the coccolith fragment. Altered surfaces may be a result of diagenetic processes in the reservoir or experimental flooding processes. Surface locations dominated by calcite are possible sites of calcite dissolution or potential calcite reprecipitation which is a common process during diagenesis [15]. In the analyzed ROIs, clay mineral phases are detected mainly as sub-micron sized particles filling cracks, adhering to the coccolith surface, or as sheetlike features.

Imaging and chemical identification by HIM-SIMS allows to identify nanosized mineral phases chemically and provides high-quality, both topographical and chemical, images. Identification of primary or secondary minerals on this scale is important for interpretation regarding wettability. Most of these phases are not possible to distinguish using SEM-EDS, hence, erroneous conclusions may be drawn. HIM results will clearly identify locations where mineral phases cover the coccolith, and the combination with SIMS will additionally provide chemical information and confirm the presence of non-carbonate phases, such as clay minerals (Figure 5a). However, when acquiring data for mass m/z 56, in the attempt to map ^{56}Fe, it is ambiguous, as the SIMS system (providing a mass resolution power m/Δm $\approx$ 400) [33], could not differentiate the compound ^{40}Ca ^{16}O from ^{56}Fe due to mass interference (mass resolution of at least 2500 necessary). Glauconite (K,Na)(Fe^{3+},Al,Mg)$_2$(Si,Al)$_4$O$_{10}$(OH)$_2$ is present in St. Vaast Formation [28] and is likely to be identified in this sample, besides the presence of 0.4 wt.% Fe (Table 1) can enhance the probability of glauconite presence. Based on shape and data acquired by SIMS, the mineral phase identified is more likely illite (K,H$_3$O)(Al,Mg,Fe)$_2$(Si,Al)$_4$O$_{10}$[(OH)$_2$·(H$_2$O)].

MgO was the only element that was enriched in the sample during the flooding experiment, showing values of 0.4–0.6 wt.% after flooding compared to <0.3 wt.% in unflooded samples. The increase in Mg^{2+} has been demonstrated in numerous flooding experiments, leading to growth of magnesite [9,10]. In the ROI studied with HIM-SIMS (Figure 4e) magnesite ($MgCO_3$) could not be identified. The increased amount of Mg^{2+} (Table 1), derived from the injected fluid, is possibly retained in the sample by increasing the magnesium concentration in present clay minerals. However, this requires further studies on clays before and after flooding experiments. Two clay minerals identified with different shapes (Figure 6) may have different concentrations of magnesium. By comparing the distribution of ^{24}Mg versus ^{27}Al, ^{28}Si, and ^{39}K for 6d-c and 6h-g it is likely that the clay mineral in 6h has a higher ^{24}Mg concentration. SIMS may nevertheless not reflect accurate quantification and additional data, either with the use of standards or by a different method, is needed.

6. Conclusions

An Upper Cretaceous outcrop chalk sample, where calcite is the most abundant phase (up to 95 %) with an artificial fracture of a diameter of 2.25 ($\pm$0.05) mm, was flooded by SSW under reservoir conditions (T = 130 $^\circ$C; p = 12 MPa) at the Norwegian Continental Shelf over approximately two months. This is a routine experiment regarding IOR research [2,9]. Mg^{2+} is one of the most reactive ions in SSW and the sample increased the bulk MgO concentration from 0.28 to 0.52 wt.% (Table 1) as expected, e.g., [9,37]. The combination of high-resolution SE imaging by HIM combined with elemental maps obtained by SIMS, showed that calcite was in numerous areas covered by other phases, challenging to resolve with traditional analytical methods such as SEM-EDS. In various research studies within this field, this observation had not previously been described or monitored ([9,10]) wherefore the presented study is novel and highlights the need of such analytical approach. In our case study, we could show that the HIM can identify phases covering the coccolith surface thoroughly and that high-resolution SIMS imaging allowed us to characterize those phases chemically which is the major advance using the combined HIM-SIMS. Moreover, most of the phases can be identified with chemical tools and, in cases, a secondary nature can even be interpreted. This has tremendous impact on further aspects of wettability processes and imbibition, as we can now show that calcite surfaces are heterogeneously covered by other mineral phases. These are novel data for modeling of wettability or other rock–fluid interaction processes. HIM-SIMS is a highly recommended method in reservoir characterization of fine-grained rocks when key processes take place on sub-micron and even nano-scale level. Moreover, sample preparation is very rapid, similar to traditional SEM-EDS studies. Hence, this technique, HIM-SIMS, opens new horizons for a variety of research fields within IOR and petroleum geosciences.

References

1. Scholle, P.A.; Hsu, K.; Jenkyns, H. Diagenesis of Upper Cretaceous chalks from England, Northern Ireland and the North Sea. In *Pelagic Sediments: On Land and under the Sea*; John Wiley & Sons, Inc.: Hoboken, NJ, USA, 1974; pp. 177–210.
2. Strand, S.; Standnes, D.C.; Austad, T. Spontaneous Imbibition of Aqueous Surfactant Solutions into Neutral to Oil-Wet Carbonate Cores: Effects of Brine Salinity and Composition. *Energy Fuels* **2003**, *17*, 1133–1144. [CrossRef]
3. Korsnes, R.I.; Strand, S.; Hoff, Ø.; Pedersen, T.; Madland, M.V.; Austad, T. Does the chemical interaction between seawater and chalk affect the mechanical properties of chalk?. In *Eurock 2006: Multiphysics Coupling and Long Term Behaviour in Rock Mechanics*; Taylor & Francis: London, UK, 2006; pp. 427–434. ISBN 00415410010.
4. Korsnes, R.; Madland, M.V.; Austad, T. Impact of brine composition on the mechanical strength of chalk at high Temperature. In *Eurock 2006: Multiphysics Coupling and Long Term Behaviour in Rock Mechanics*; Taylor & Francis: London, UK, 2006; pp. 133–140, ISBN 0415410010.
5. Zhang, P.; Tweheyo, M.T.; Austad, T. Wettability alteration and improved oil recovery by spontaneous imbibition of seawater into chalk: Impact of the potential determining ions Ca^{2+}, Mg^{2+}, and $SO4^{2-}$. *Colloids Surf. A Physicochem. Eng. Asp.* **2007**, *301*, 199–208. [CrossRef]
6. Madland, M.V.; Midtgarden, K.; Manafov, R. The effect of temperature and brine composition on the mechanical strength of Kansas chalk. In Proceedings of the International Symposium of the Society of Core Analysts, Abu Dhabi, United Arab Emirates, 29 October–2 November 2008; p. 6.
7. Newman, G.H. The Effect of Water Chemistry on the Laboratory Compression and Permeability Characteristics of Some North Sea Chalks. *J. Pet. Technol.* **1983**, *35*, 976–980. [CrossRef]
8. Nermoen, A.; Korsnes, R.; Aursjø, O.; Madland, M.; Kjørslevik, T.A.; Østensen, G. How Stress and Temperature Conditions Affect Rock-Fluid Chemistry and Mechanical Deformation. *Front. Phys.* **2016**, *4*. [CrossRef]
9. Andersen, P.Ø.; Wang, W.; Madland, M.V.; Zimmermann, U.; Korsnes, R.I.; Bertolino, S.R.A.; Minde, M.; Schulz, B.; Gilbricht, S. Comparative Study of Five Outcrop Chalks Flooded at Reservoir Conditions: Chemo-mechanical Behaviour and Profiles of Compositional Alteration. *Transp. Porous Media* **2018**, *121*, 135–181. [CrossRef]
10. Zimmermann, U.; Madland, M.V.; Nermoen, A.; Hildebrand-Habel, T.; Bertolino, S.A.R.; Hiorth, A.; Korsnes, R.I.; Audinot, J.-N.; Grysan, P. Evaluation of the compositional changes during flooding of reactive fluids using scanning electron microscopy, nano-secondary ion mass spectrometry, x-ray diffraction, and whole-rock geochemistryCompositional Changes during Flooding. *AAPG Bull.* **2015**, *99*, 791–805. [CrossRef]
11. Megawati, M.; Andersen, P.Ø.; Korsnes, R.I.; Evje, S.; Hiorth, A.; Madland, M.V. The Effect of Aqueous Chemistry pH on the Time-Dependent Deformation Behaviour of Chalk-Experimental and Modelling Study. In Proceedings of the Pore2Fluid International IFP Energies Nouvelles, Paris, France, 16–18 November 2011.
12. Hellmann, R.; Renders, P.; Gratier, J.; Guiguet, R. Experimental pressure solution compaction of chalk in aqueous solutions Part 1. Deformation behavior and chemistry. In *Water–Rock Interactions, Ore Deposits, and Environmental Geochemistry*; Hellmann, R., Wood, S.A., Eds.; Geochemical Society: Washington, DC, USA, 2002; Volume 7, pp. 129–152.
13. Madland, M.V.; Hiorth, A.; Omdal, E.; Megawati, M.; Hildebrand-Habel, T.; Korsnes, R.I.; Evje, S.; Cathles, L.M. Chemical Alterations Induced by Rock–Fluid Interactions When Injecting Brines in High Porosity Chalks. *Transp. Porous Media* **2011**, *87*, 679–702. [CrossRef]
14. Fabricius, I.L.; Borre, M.K. Stylolites, porosity, depositional texture, and silicates in chalk facies sediments. *Ontong Java-Plateau—Gorm Tyra Fields North Sea Sedimentol.* **2007**, *54*, 183–205.
15. Hjuler, M.L.; Fabricius, I.L. Engineering properties of chalk related to diagenetic variations of Upper Cretaceous onshore and offshore chalk in the North Sea area. *J. Pet. Sci. Eng.* **2009**, *68*, 151–170. [CrossRef]
16. Megawati, M.; Madland, M.V.; Hiorth, A. Mechanical and physical behavior of high-porosity chalks exposed to chemical perturbation. *J. Pet. Sci. Eng.* **2015**, *133*, 313–327. [CrossRef]
17. Zimmermann, U.; Madland, M.V.; Minde, M.; Borromeo, L.; Egeland, N. Tools to Determine and Quantify Mineralogical Changes During EOR Flooding Experiments on Chalk. In Proceedings of the Abu Dhabi International Petroleum Exhibition & Conference, Abu Dhabi, United Arab Emirates, 13–16 November 2017.
18. Priebe, A.; Barnes, J.-P.; Edwards, T.E.J.; Pethö, L.; Balogh, I.; Michler, J. 3D Imaging of Nanoparticles in an Inorganic Matrix Using TOF-SIMS Validated with STEM and EDX. *Anal. Chem.* **2019**, *91*, 11834–11839. [CrossRef] [PubMed]
19. Notte, J.; Goetze, B. Imaging with the Helium Ion Microscope. In *Surface Analysis and Techniques in Biology*; Smentkowski, V.S., Ed.; Springer International Publishing: Cham, Switzerland, 2014; pp. 171–194.
20. Minde, M.W.; Zimmermann, U.; Madland, M.V.; Korsnes, R.I.; Schulz, B.; Gilbricht, S. Mineral Replacement in Long-Term Flooded Porous Carbonate Rocks. *Geochim. Cosmochim. Acta* **2019**, *268*, 485–508. [CrossRef]

21. Minde, M.W.; Madland, M.V.; Zimmermann, U.; Egeland, N.; Korsnes, R.I.; Nakamura, E.; Kobayashi, K.; Ota, T. Mineralogical alterations in calcite powder flooded with $MgCl_2$ to study Enhanced Oil Recovery (EOR) mechanisms at pore scale. *Microporous Mesoporous Mater.* **2019**, *304*, 109402. [CrossRef]

22. Borromeo, L.; Egeland, N.; Minde, M.W.; Zimmermann, U.; Andò, S.; Madland, M.V.; Korsnes, R.I. Quick, Easy, and Economic Mineralogical Studies of Flooded Chalk for EOR Experiments Using Raman Spectroscopy. *Minerals* **2018**, *8*, 221. [CrossRef]

23. Audinot, J.-N.; Philipp, P.; De Castro, O.; Biesemeier, A.; Hoang, Q.H.; Wirtz, T. Highest resolution chemical imaging based on secondary ion mass spectrometry performed on the helium ion microscope. Reports on progress in physics. *Rep. Prog. Phys.* **2021**, *84*, 105901. [CrossRef]

24. Wirtz, T.; De Castro, O.; Audinot, J.-N.; Philipp, P. Imaging and Analytics on the Helium Ion Microscope. *Annu. Rev. Anal. Chem.* **2019**, *12*, 523–543. [CrossRef]

25. Schroeder, C.; Gaviglio, P.; Bergerat, F.; Vandycke, S.; Coulon, M. Faults and matrix deformations in chalk: Contribution of porosity and sonic wave velocity measurements. *Bull. Soc. Geol. Fr.* **2006**, *177*, 203–213. [CrossRef]

26. Dusar, M.; Lagrou, D. Cretaceous flooding of the Brabant Massif and the lithostratigraphic characteristics of its chalk cover in northern Belgium. *Geol. Belg.* **2007**, *10*, 27–38.

27. Robaszynski, F.; Dhondt, A.; Jagt, J. Cretaceous lithostratigraphic units (Belgium). *Geol. Belg.* **2001**, *4*, 121–134. [CrossRef]

28. Briart, F.L.C. Saint-Vaast Chalk Formation—SVA. 2000. Available online: https://ncs.naturalsciences.be/cretaceous/2114-saint-vaast-chalk-formation-sva (accessed on 7 January 2022).

29. Abubeker, E. Water Weakening of Chalks—Comparsion of Intact and Fractured Cores. Master's Thesis, Faculty of Science and Technology, University of Stavanger, Stavanger, Norway, 2013; p. 88. Available online: https://uis.brage.unit.no/ (accessed on 13 December 2021).

30. Geitle, K. Chemically Induced Compaction in Fractured and Intact Chalk Cores. Master's Thesis, Institute for Energy and Resources (IER), University of Stavanger, Stavanger, Norway, 2013; p. 78. Available online: https://uis.brage.unit.no/uis (accessed on 13 December 2021).

31. Hlawacek, G.; Gölzhäuser, A. (Eds.) *Helium Ion Microscopy*; Springer International Publishing: Cham, Switzerland, 2016; p. 526.

32. Pillatsch, L.; Vanhove, N.; Dowsett, D.; Sijbrandij, S.; Notte, J.; Wirtz, T. Study and optimisation of SIMS performed with He^+ and Ne^+ bombardment. *Appl. Surf. Sci.* **2013**, *282*, 908–913. [CrossRef]

33. Dowsett, D.; Wirtz, T. Co-registered in situ secondary electron and mass spectral imaging on the helium ion microscope demonstrated using lithium titanate and magnesium oxide nanoparticles. *Anal. Chem.* **2017**, *89*, 8957–8965. [CrossRef] [PubMed]

34. Kim, S.; Trofimov, A.; Khanom, F.; Stern, L.; Lamberti, W.; Colby, R.; Abmayr, D.; Belianinov, A.; Ovchinnikova, O.S. High Resolution Multimodal Chemical Imaging Platform for Organics and Inorganics. *Anal. Chem.* **2019**, *91*, 12142–12148. [CrossRef] [PubMed]

35. Vollnhals, F.; Wirtz, T. Correlative Microscopy in 3D: Helium Ion Microscopy-Based Photogrammetric Topography Reconstruction Combined with in situ Secondary Ion Mass Spectrometry. *Anal. Chem.* **2018**, *90*, 11989–11995. [CrossRef] [PubMed]

36. Ost, A.D.; Wu, T.; Höschen, C.; Mueller, C.W.; Wirtz, T.; Audinot, J.-N. 4D Surface Reconstructions to Study Microscale Structures and Functions in Soil Biogeochemistry. *Environ. Sci. Technol.* **2021**, *55*, 9384–9393. [CrossRef] [PubMed]

37. Minde, M.W.; Wang, W.; Madland, M.V.; Zimmermann, U.; Korsnes, R.I.; Bertolino, S.R.; Andersen, P. Temperature effects on rock engineering properties and rock-fluid chemistry in opal-CT-bearing chalk. *J. Pet. Sci. Eng.* **2018**, *169*, 454–470. [CrossRef]